

Discovery of ordered and quasi-ordered photonic crystal structures in the scales of the beetle *Eupholus magnificus*

C. Pouya,^{1*} D. G. Stavenga² and P. Vukusic¹

¹*School of Physics, University of Exeter, Exeter, EX4 4QL, UK*

²*Department of Neurobiophysics, University of Groningen, Groningen, Netherlands*

*C.Pouya@exeter.ac.uk

Abstract: The outer wing casings (elytra) of the weevil *Eupholus magnificus* are marked by yellow and blue bands. We have investigated the scales covering the elytra by using microspectrophotometry, imaging scatterometry, scanning electron microscopy and Fourier transform analysis. We demonstrate that the scales in the yellow elytral bands comprise highly ordered 3D photonic crystal structures, whereas the scales of the blue bands comprise quasi-ordered 3D photonic structures. Both systems, highly contrasting in their periodic order, create approximately angle-independent colour appearances in the far-field. The co-existence of these two contrasting forms of 3D structural order in the same single species is certainly uncommon in natural biological systems and has not been reported in the photonic literature.

©2011 Optical Society of America

OCIS codes: (160.1435) Biomaterials; (160.5293) Photonic bandgap materials; (160.5298) Photonic crystals.

References and links

1. J. D. Joannopoulos, S. G. Johnson, J. N. Winn, and R. D. Meade, *Photonic Crystals: Molding the Flow of Light* (Second Edition) (Princeton University Press, Princeton, NJ, 2008).
2. J. C. Knight, J. Broeng, T. A. Birks, and P. S. J. Russell, "Photonic band gap guidance in optical fibers," *Science* **282**(5393), 1476–1478 (1998).
3. J. Jágerská, H. Zhang, Z. Diao, N. L. Thomas, and R. Houdré, "Refractive index sensing with an air-slot photonic crystal nanocavity," *Opt. Lett.* **35**(15), 2523–2525 (2010).
4. H. Altug, D. Englund, and J. Vučković, "Ultrafast photonic crystal nanocavity laser," *Nat. Phys.* **2**(7), 484–488 (2006).
5. D. Levine, and P. Steinhardt, "Quasicrystals: A New Class of Ordered Structures," *Phys. Rev. Lett.* **53**(26), 2477–2480 (1984).
6. M. Zoorob, M. Charlton, G. Parker, J. Baumberg, and M. Netti, "Complete and absolute photonic bandgaps in highly symmetric photonic quasicrystals embedded in low refractive index material," *Mater. Sci. Eng. B* **74**(1-3), 168–174 (2000).
7. H. Huang, C. H. Lin, Z. K. Huang, K. Y. Lee, C. C. Yu, and H. C. Kuo, "Double Photonic Quasi-Crystal Structure Effect on GaN-Based Vertical-Injection Light-Emitting Diodes," *Jpn. J. Appl. Phys.* **49**(2), 022101 (2010).
8. A. Parker, D. McKenzie, and M. Large, "Multilayer reflectors in animals using green and gold beetles as contrasting examples," *J. Exp. Biol.* **201**, 1307–1313 (1998).
9. P. Vukusic, and J. R. Sambles, "Photonic structures in biology," *Nature* **424**(6950), 852–855 (2003).
10. K. Kertész, Z. Bálint, Z. Vértésy, G. I. Márk, V. Lousse, J. P. Vigneron, M. Rassart, and L. P. Biró, "Gleaming and dull surface textures from photonic-crystal-type nanostructures in the butterfly *Cyanophrys remus*," *Phys. Rev. E Stat. Nonlin. Soft Matter Phys.* **74**(2), 021922 (2006).
11. L. Biró, K. Kertész, Z. Vértésy, G. Mark, Z. Bálint, V. Lousse, and J. Vigneron, "Living photonic crystals: Butterfly scales — Nanostructure and optical properties," *Mater. Sci. Eng. C* **27**, 941–946 (2007).
12. J. W. Galusha, L. R. Richey, J. S. Gardner, J. N. Cha, and M. H. Bartl, "Discovery of a diamond-based photonic crystal structure in beetle scales," *Phys. Rev. E Stat. Nonlin. Soft Matter Phys.* **77**(5), 050904 (2008).
13. M. Srinivasarao, "Nano-Optics in the Biological World: Beetles, Butterflies, Birds, and Moths," *Chem. Rev.* **99**(7), 1935–1962 (1999).
14. S. Kinoshita, *Structural Colours in the Realm of Nature* (World Scientific, Singapore, 2008).

15. O. Deparis, C. Vandenbem, M. Rassart, V. Welch, and J. P. Vigneron, "Color-selecting reflectors inspired from biological periodic multilayer structures," *Opt. Express* **14**(8), 3547–3555 (2006).
16. J. A. Noyes, P. Vukusic, and I. R. Hooper, "Experimental method for reliably establishing the refractive index of buprestid beetle exocuticle," *Opt. Express* **15**(7), 4351–4358 (2007).
17. S. Kinoshita, S. Yoshioka, Y. Fujii, and N. Okamoto, "Photophysics of structural color in the Morpho butterflies," *Forma* **17**, 103–121 (2002).
18. E. J. Denton, "Reflectors in fishes," *Sci. Am.* **224**(1), 64–72 (1971).
19. T. M. Trzeciak, and P. Vukusic, "Photonic crystal fiber in the polychaete worm *Pherusa* sp.," *Phys. Rev. E Stat. Nonlin. Soft Matter Phys.* **80**(6), 061908 (2009).
20. K. Michielsen, and D. G. Stavenga, "Gyroid cuticular structures in butterfly wing scales: biological photonic crystals," *J. R. Soc. Interface* **5**(18), 85–94 (2008).
21. K. Michielsen, H. De Raedt, and D. G. Stavenga, "Reflectivity of the gyroid biophotonic crystals in the ventral wing scales of the Green Hairstreak butterfly, *Callophrys rubi*," *J. R. Soc. Interface* **7**(46), 765–771 (2010).
22. P. Vukusic, B. Hallam, and J. Noyes, "Brilliant whiteness in ultrathin beetle scales," *Science* **315**(5810), 348 (2007).
23. J. P. Vigneron, M. Rassart, Z. Vértessy, K. Kertész, M. Sarrazin, L. P. Biró, D. Ertz, and V. Lousse, "Optical structure and function of the white filamentary hair covering the edelweiss bracts," *Phys. Rev. E Stat. Nonlin. Soft Matter Phys.* **71**(1), 011906 (2005).
24. D. G. Stavenga, H. L. Leertouwer, P. Pirih, and M. F. Wehling, "Imaging scatterometry of butterfly wing scales," *Opt. Express* **17**(1), 193–202 (2009).
25. P. Vukusic, and D. G. Stavenga, "Physical methods for investigating structural colours in biological systems," *J. R. Soc. Interface* **6**(Suppl 2), S133–S148 (2009).
26. V. Sharma, M. Crne, J. O. Park, and M. Srinivasarao, "Structural origin of circularly polarized iridescence in jeweled beetles," *Science* **325**(5939), 449–451 (2009).
27. A. E. Seago, P. Brady, J. P. Vigneron, and T. D. Schultz, "Gold bugs and beyond: a review of iridescence and structural colour mechanisms in beetles (Coleoptera)," *J. R. Soc. Interface* **6**(Suppl 2), S165–S184 (2009).
28. V. Saranathan, C. O. Osuji, S. G. J. Mochrie, H. Noh, S. Narayanan, A. Sandy, E. R. Dufresne, and R. O. Prum, "Structure, function, and self-assembly of single network gyroid (I4132) photonic crystals in butterfly wing scales," *Proc. Natl. Acad. Sci. U.S.A.* **107**(26), 11676–11681 (2010).
29. M. C. Hutley, *Diffraction Gratings*, Techniques of Physics **6** (Academic Press, London, 1982).
30. A. Okabe, B. Boots, K. Sugihara, and S. N. Chiu, *Spatial Tessellations-Concepts and Applications of Voronoi Diagrams* (Second Edition). (John Wiley and Sons, Chichester, 2000).
31. A. P. Li, F. Müller, and U. Gösele, "Electrochem. Polycrystalline and Monocrystalline Pore Arrays with Large Interpore Distance in Anodic Alumina," *Solid-St.* **3**, 155112 (2000).
32. R. O. Prum, and R. H. Torres, "Structural colouration of mammalian skin: convergent evolution of coherently scattering dermal collagen arrays," *J. Exp. Biol.* **207**(12), 2157–2172 (2004).
33. M. Florescu, S. Torquato, and P. Steinhardt, "Complete band gaps in two-dimensional photonic quasicrystals," *Phys. Rev. B* **80**(15), 155112 (2009).
34. P. Vukusic, and J. R. Sambles, "Shedding light on butterfly wings" *Proc. SPIE* **4438**, 0277–786X/01 (2001).
35. C. C. Cheng, and A. Scherer, "New fabrication techniques for high quality photonic crystals," *J. Vac. Sci. Technol. B* **15**(6), 2764–2767 (1997).
36. H. T. Miyazaki, H. Miyazaki, K. Ohtaka, and T. Sato, "Photonic band in two-dimensional lattices of micrometer-sized spheres mechanically arranged under a scanning electron microscope," *J. Appl. Phys.* **87**(10), 7152–7158 (2000).
37. I. Divliansky, T. S. Mayer, K. S. Holliday, and V. H. Crespi, "Fabrication of three-dimensional polymer photonic crystal structures using single diffraction element interference lithography," *Appl. Phys. Lett.* **82**(11), 1667 (2003).
38. M. Deubel, G. von Freymann, M. Wegener, S. Pereira, K. Busch, and C. M. Soukoulis, "Direct laser writing of three-dimensional photonic-crystal templates for telecommunications," *Nat. Mater.* **3**(7), 444–447 (2004).
39. M. S. Rill, C. Plet, M. Thiel, I. Staude, G. von Freymann, S. Linden, and M. Wegener, "Photonic metamaterials by direct laser writing and silver chemical vapour deposition," *Nat. Mater.* **7**(7), 543–546 (2008).
40. T. Ding, K. Song, K. Clays, and C. H. Tung, "Fabrication of 3D Photonic Crystals of Ellipsoids: Convective Self-Assembly in Magnetic Field," *Adv. Mater.* **21**(19), 1936–1940 (2009).
41. B. Hatton, L. Mishchenko, S. Davis, K. H. Sandhage, and J. Aizenberg, "Assembly of large-area, highly ordered, crack-free inverse opal films," *Proc. Natl. Acad. Sci. U.S.A.* **107**(23), 10354–10359 (2010).

1. Introduction

Photonic crystals (PCs) have been the subject of rapidly increasing interest over recent years [1]. They offer the potential for use in many optics-based applications due, principally, to their ability to shape and control the flow of light and colour [2–4]. While the periodic structure of highly ordered photonic crystals creates strong light manipulation, the structural nature of quasi-ordered crystals that show higher orders of rotational symmetry is attracting increasing interest from the photonics community. Such quasi-ordered crystals are not limited

by the same geometric constraints with which ordered structures are restricted. For this reason they can exhibit higher orders of rotational symmetry [5] therefore producing a more spherical Brillouin zone. The structure that offers the most spherical Brillouin zone of all the ordered 3D PCs is the diamond structure. It must comprise materials that contribute to a minimum refractive index contrast of ~ 2 to exhibit a full and complete photonic band-gap (FCPBG). Fabrication of FCPBG structures therefore demands careful choice of suitably high refractive index materials. However, the more isotropic nature of quasi-ordered PCs offers the potential advantage of a more spherical Brillouin zone than an ordered PC. The possibility for complete photonic band-gap generation, using materials that have a lower refractive index contrast, therefore becomes available, making fabrication and compatibility of complete photonic band-gap devices more accessible [6]. This will allow the design of specific optical properties with the knowledge that only a low refractive index contrast is necessary. Many applications including LEDs can utilise the many properties associated with quasi-ordered PCs: in the case of LEDs, quasi-ordered PCs may be used to enhance the extraction efficiency by reducing the absorption of reflected light [7].

Since the emergence of photonic crystal physics approximately two decades ago [1] the light manipulation potential associated with photonic crystal systems has been the subject of significant experimental and theoretical examination [8–12]. It has since been recognised that the biological world has evolved a vast array of photonic crystal systems each of which serve light manipulation purposes and thereby create and control a grand diversity of visible appearances [9, 13, 14]. For instance, butterflies, beetles, birds and even aquatic systems utilize the optical properties of one, two, and three-dimensional photonic crystals to enhance and control display or crypsis [12–14]. One-dimensional systems include the multilayer structure of many species of beetle [8, 15, 16], butterflies [17] and fish [18]. Two-dimensional structures include the two-dimensional hexagonal structure found in the polychaete worm [19]. Three-dimensional inverse opal structures and even more elaborate structures including bicontinuous gyroids have also been found in many beetles and butterflies [10, 20, 21]. Three-dimensional structures comprising disordered arrays of filaments have also been shown to produce brilliant whiteness in other biological systems [22, 23]. This wide variety of natural photonic structures each serves a specific functional purpose.

Here we report our investigation of the weevil *Eupholus magnificus* (Fig. 1). The elytra of this weevil are marked by distinct yellow and blue coloured bands. The colours originate from assemblies of coloured scales that cover the exoskeleton. Initial visual inspection revealed that the colours are not pigmentary, but have structural bases. They were investigated with high resolution electron microscopy. These intro-scale structures were found to be three dimensional in nature. Entirely surprisingly, they comprised two very different extents of structural order. The characteristics of this variation in 3D crystal order, and the photonic properties they conferred to their associated coloured band region, is the subject of this investigation. We used a variety of techniques to understand the photonics of the nanostructures that cause the colour of these scales and their associated elytral bands.

2. Methods

Reflectance spectra of larger elytral regions of *E. magnificus* (Fig. 1(a)), comprising many juxtaposed scales, were measured with a bifurcated fibre-optic probe connected to a CCD detector array spectrometer (AvaSpec-2048, Avantes, Eerbeek, The Netherlands), using a deuterium/halogen light source (AvaLight-D(H)-S). A white diffuse reference tile (Avantes WS-2) served as reference standard [24].

Reflectance spectra of the areas within individual scales of the different coloured regions were acquired with a microspectrophotometer (MSP). This method comprised a xenon light source, a Leitz Ortholux microscope and an S2000 fibre optic spectrometer (Ocean Optics). The microscope objective was an Olympus 20x, NA 0.46.

The far-field scattering patterns of the different coloured regions of *E. magnificus* were investigated with an imaging scatterometer that captures the full hemispherical scattering pattern of an illuminated sample [24, 25]. The scattering pattern provides evidence of optical phenomena such as directionality and diffraction that arise due to the nature of the sample. Small elytral regions, each cut from the yellow and blue elytral bands, were in turn glued to the tip of separate glass micropipettes, which were mounted on a micromanipulator. This enabled positioning of a scale at one of the focal points of the scatterometer's ellipsoidal mirror. A white light beam was focused at a chosen point on the sample, invariably within the area occupied by a single elytral scale. The light scattered by the scale, and subsequently reflected by the ellipsoidal mirror, was captured via an imaging system using a digital camera. The captured images were processed as polar plots (for further details see Ref [24].).

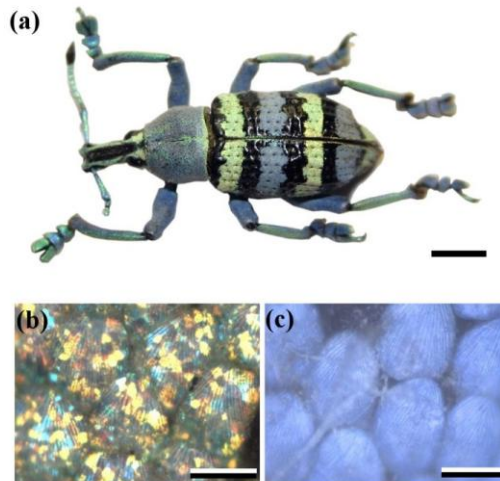


Fig. 1. (a) The weevil *Eupholus magnificus*. The elytra are marked by yellow and blue bands, with a diameter of a few mm, due to differently coloured scales. The coloured stripes alternate with dark bands where there are no scales present on the weevil's elytra: bar 4 mm. (b) Epi-illumination of the scales in the yellow elytral bands shows highly domained scales: bar 50 μm . (c) The scales in the blue bands are more or less homogenous in coloration: bar 50 μm .

The photonic nanostructures contained within the weevil scales were investigated using scanning electron microscopy (SEM) in conjunction with focused ion beam (FIB) milling (FEI Nova 600 dual-beam system; elytral samples coated with 4nm of AuPd). The Gallium ion beam used was set at a voltage of 30kV and current of 10pA to expose sections through individual scales. This approach has also been used successfully in a study of other weevil species [12].

The nature of the order and periodicity of the photonic nanostructures contained within the elytral scales was analysed by applying Fourier transform analysis on 2-D images of FIB treated cross-sections that were captured from the SEM. The extent of order, quasi-order and disorder in each sample was characterized using Voronoi analysis [26] of their associated SEM images and by applying entropy considerations.

3. Results

Light-microscopic observation of the scales in the yellow and blue elytral regions of the weevil *E. magnificus* (Fig. 1(a)) revealed that the scales distinctly differ in visual appearance. The scales from the yellow region have a domained configuration (Fig. 1(b)), whereas the scales in the blue region are largely homogeneously coloured (Fig. 1(c)).

We measured the reflectance spectra of the two differently coloured elytral regions, containing multiple scales, with a bifurcated-probe spectrophotometer, yielding spectra peaking at about 600 and 400 nm for the yellow and blue regions, respectively (Fig. 2(a)). The overall reflectance of the yellow region is in fact the superposition of the reflectances of several intra-scale domains (Fig. 1(b)), as is demonstrated by the reflectance spectra measured from individual domains within the yellow scales, performed with an epi-illumination microspectrophotometer (MSP; Fig. 2(b)). The reflectance spectra of the various domains have a bandwidth (FWHM) of about 100 nm and the peak wavelength can vary from 400 to 600 nm.

The domains are very small, some being as low as 1 μm in diameter, and therefore a very small measurement spot is required to measure from only one domain. Sometimes this cannot be achieved, as shown by the violet dashed curve in Fig. 2(b), which shows two peaks.

MSP on different areas of blue scales always yielded the same spectrum as is shown by Fig. 2(c), which presents MSP spectra from a blue scale after consecutive 2° rotation steps. The wavelength of maximum reflectance is relatively angle-independent, changing by only 10 nm after 48° of rotation (Fig. 2(c)). Because this will not result in a noticeable colour change to an observer, the reflections from the blue scales result in an angle-independent blue reflection. Interestingly, the average superposition of reflections from many differently coloured domains in the yellow scales also gives the appearance of angle-independent reflection.

The yellow and blue scales not only differ in spectral but also in spatial reflectance characteristics. We performed imaging scatterometry to investigate the spatial dependence of the light scattered by the yellow and blue scales (Fig. 3). The scales were illuminated with a narrow aperture ($\sim 5^\circ$) light beam, via a small, axial hole in the ellipsoidal mirror of the scatterometer. Illumination of single domains of the yellow scales yielded very different far-field scattering patterns compared to the blue scales. Each single domain within the yellow scales exhibited some directionality (Fig. 3(a)). Rotation of the yellow scales in steps of 10° , keeping the illumination constant, resulted not only in changing direction angles of directionally scattered light, but also in peak wavelength shifts. In contrast to this, the blue scales exhibited no directionality (Fig. 3(b)) and produced quite diffuse scattering patterns covering the whole hemispherical, polar plot.

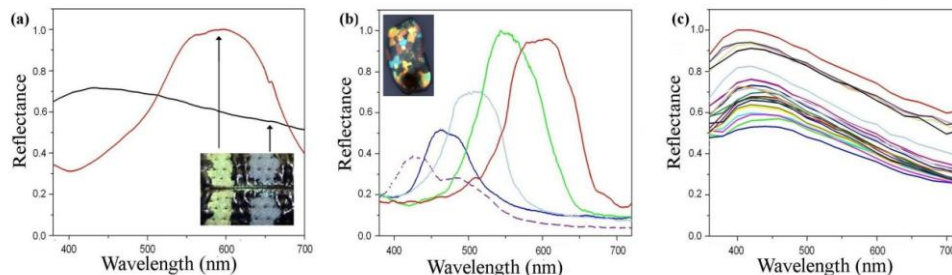


Fig. 2. Reflectance spectra of *E. magnificus*. (a) Spectra obtained from an area of the yellow (red curve) and blue (black curve) band of the elytra (inset), measured with a bifurcated probe spectrophotometer. (b) Epi-illumination microspectrophotometry (MSP) of various domains of a yellow scale (inset: a yellow scale showing the many coloured domains). (c) MSP of a blue scale rotated in steps of 2° .

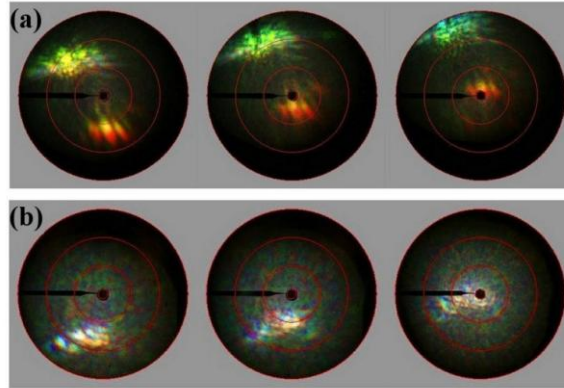


Fig. 3. Scattering patterns from the yellow (a) and blue (b) scales of *E. magnificentus*. From left to right the scales were rotated in steps of 10° (the red rings represent scattering angles of 5° , 30° , 60° and 90°).

Detailed high resolution SEM was undertaken on the scales of both coloured regions to identify the various nanostructure types that were present within their colour producing scales. SEM images revealed that the upper surface of both the yellow and the blue scales have relatively periodic ridges (Fig. 4(a), (c)). The ridges have a pitch of $1.6\text{--}3.2\ \mu\text{m}$ depending on the location on the surface of the scale. The ridge depth of the yellow scales is $\sim 2\ \mu\text{m}$ deep and of the blue scales $\sim 0.8\ \mu\text{m}$. The cross-sections from the yellow scales (Fig. 4(b)) show a highly periodic photonic crystal structure arranged in domains with clear boundaries between them. Photonic crystal domains are not unique to *E. magnificentus*: they are also found in other weevil species [12, 27] and in many butterflies [9, 20, 28]. The juxtaposed intra-scale domains of photonic crystal in this species create the individual neighbouring yellow, green and blue colour centres observable in the optical image shown in Fig. 1(b). Occasionally, an individual PC domain will lie on top of a neighbouring domain, rather than simply horizontally adjacent to it (Fig. 4(b)). This creates an additive colour mixing process from within a single observed intra-scale domain region. It will be measured as a double-peak reflection captured from within a single apparent colour domain region (Fig. 2(b) – violet dashed curve, showing reflection maxima at $430\ \text{nm}$ and $485\ \text{nm}$).

The sections from the homogeneously coloured blue scales (Fig. 4(d)) also appear to show photonic crystal structures in the SEM images. However, they differ significantly from those of the yellow scales. The photonic crystal of their scales clearly lacks distinct and well-defined structural periodicity. Not only does this create an element of disorder within the scale, but it also removes the apparent presence of domaining.

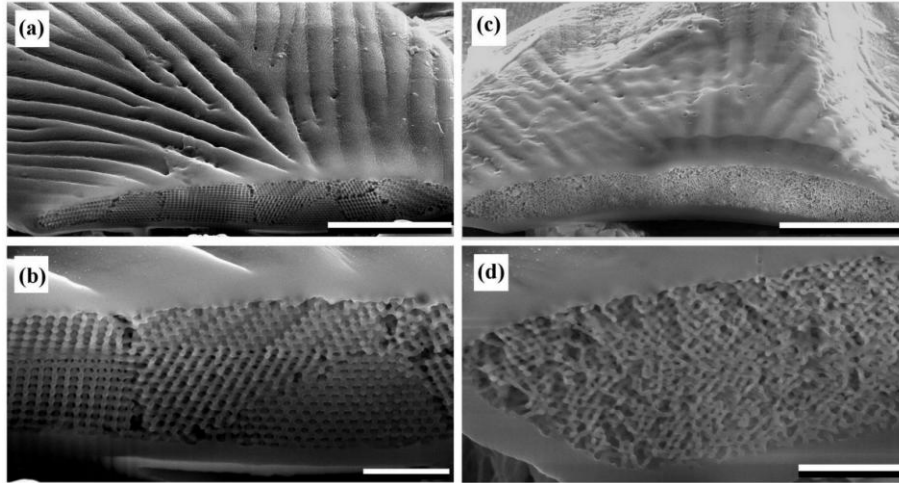


Fig. 4. SEM images of a yellow scale (a, b) and a blue scale (c, d) of *E. magnificus*, cross-sectioned using FIB milling. Below the ridged surfaces (a, c), in the yellow scale a highly ordered periodic 3D-lattice exists (b), whereas in the blue scale the lattice is quasi-ordered (d). (a, c): bar 10 μm , (b, d): bar 2 μm .

Both yellow and blue scales show evidence of diffraction. Close analysis of Fig. 3(a), for the scattered light collected from a single illuminated yellow scale, shows that the angular separation of the diffracted orders of red wavelengths is approximately 12° . The surface separation of these yellow scales have a pitch of approximately $3 \mu\text{m}$ (Fig. 4 (a)). The grating equation [29] confirms that the surface ridging is directly responsible for this. Since this is the diffraction collected from interrogation of a single scale surface, it will not be resolved or discernable when the incident beam spot encompasses multiple scales over a much larger area.

Voronoi analysis was applied to high resolution SEM images of each scale type's structure. This generated information associated with the number of nearest neighbours of each lattice point within the images' fields of view by creating what is known as a Voronoi diagram [30]. Following this, the extent of each scale's photonic structure was quantified using entropy (S) considerations, using the equation:

$$S = \frac{\sum P_n \ln(P_n)}{\ln(N)} \quad (1)$$

where P_n is the number of nearest neighbours or fraction of n sided shapes made by the Voronoi diagram and N is the number of different shapes in the Voronoi diagram. This method has been successfully analogously used in the analysis of other structurally coloured systems [26]. For an ordered system the entropy is expected to be $S = 0$ and for a disordered system $S = 1$. Voronoi and entropy analysis on the photonic nanostructures within the scales from the yellow (y) and blue (b) regions show entropy values of $S_y = 0$ and $S_b = 0.66$, offering a quantified measure of the very different extent of the structural order.

In order to determine the spatial frequencies of the scale's photonic crystal structures, we performed 2D Fast Fourier transforms (FFTs) on the structures from each type of coloured scale. The 2D FFT image of the yellow scale structures yielded the six-fold symmetric regular pattern (Fig. 5(a)) that is expected from the highly periodic hexagonal structure used as the image source taken from one domain. The 2D FFT image of the structure within the blue scales (Fig. 5(b)) shows a more complex intensity distribution pattern comprising two principal components. The first is a clear circle of broad intensity, equal in all directions. This indicates the prevalence of various length-scales of long range periodic order in the form of

structural polycrystallinity [31, 32]. The second intensity distribution is formed of a group of twelve short-range radially-distributed sharp intensity maxima that are positioned on the edge of the broad intensity signal. These are indicative of a very isotropic formation of a 12-fold-symmetric photonic crystal structure. Such high rotational order is consistent with a quasi-ordered crystalline structure. Florescu *et al.* presented similar intensity distributions in FFT images of quasi-ordered synthetically fabricated structures that have unusual high orders of rotational symmetry [33].

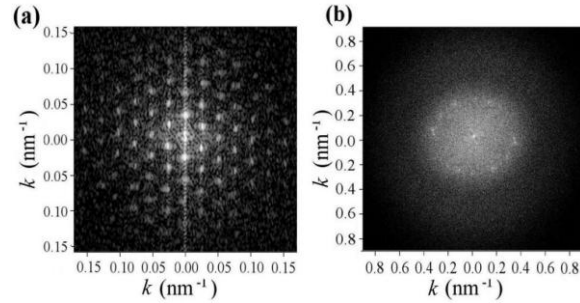


Fig. 5. Fourier transforms of the photonic nanostructures within the yellow scales (a) and blue scales (b) of *E. magnificus*.

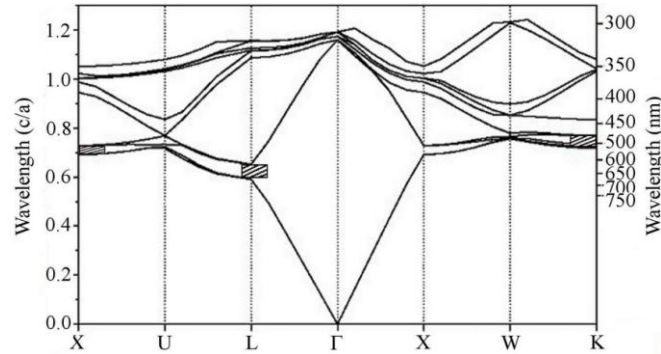


Fig. 6. Photonic band diagram of an ideal inverse FCC photonic crystal with cubic supercell length $a = 368$ nm and radius of air spheres $r = 100$ nm. The striped boxes highlight the partial band-gaps at the X, L and K points corresponding to the reflectance maxima shown in Fig. 2b.

The photonic crystal structures within the yellow scales can be considered as various orientations of a 3D inverse opal structure arranged in juxtaposed domains. The structure has a lattice constant $a = 368$ nm (cubic supercell length) and radius of air spheres $r = 100$ nm. Comparison of SEM images of the yellow scale structures to cross-sectional geometries of digitally rendered crystal structures, following previously published methods [20, 34], suggests this structure is closely related to a variation of a face-centred-cubic (FCC) lattice. While formal verification is required, it is practical to create a theoretical model of an ideal FCC structure, using the lattice parameters described earlier, of air spheres in a cuticle matrix. This was done using the MIT Photonic Bands package and yielded the band diagram shown in Fig. 6. The partial band gaps in Fig. 6 can be directly related to mid-peak reflections from the experimental optical data presented in Fig. 2(b). The wavelength gap at the X, L and K points (as labelled in Fig. 6) correspond closely to the reflectance maxima shown in Fig. 2(b).

4. Conclusion

We have identified two contrasting 3D photonic crystal structures for producing overall angle-independent colour reflection in the scales of *E. magnificus*. Groups of scales with domain-based order such as those forming the yellow scale regions, appear to contain the

same 3D structure. Each juxtaposed 3D domain comprises a variously oriented 3D crystal grain. Each individual domain of structure produces angle-dependent reflection, resulting in different spectral and spatial scattering properties. Over many domains, from many scales, the ensemble additive effect is an appearance and colouration that offers far-field angle-independence. This has been documented in other species with 3D photonic crystals [12, 20, 27, 34]. Colour averaging via such domaining is a common method for production of large area far-field angle-independent colour reflection in many beetles, possibly since the refractive index contrast of air-cuticle (~ 1.56) is too small to produce this effect. Namely, a complete photonic band gap with a single orientation of ordered 3D structure is not possible for PCs comprising materials with such a low refractive index contrast. This weevil has also adapted its photonic crystal structure to overcome the low refractive index contrast of air-cuticle systems in another way: namely, by the use of quasi-ordered, rather than highly-ordered, photonic crystal structures. Since ordered periodicities are not involved, these structures do not carry the usual geometrical constraints associated with periodic crystallographic restrictions. Quasi-ordered photonic crystal geometries therefore create a more isotropic optical scattering structure due to their relatively spherical Brillouin zone boundaries [6].

Synthetic fabrication of photonic crystal systems is well advanced [35–39] with many self-assembly processes emerging as an exciting hot-topic currently [40, 41]. However, with few exceptions [7], it is only highly ordered 3D systems that have been fabricated for the visible band. These have exhibited full and complete photonic band gap (FCPBG) properties due, largely, to the ultra-high contrast in the refractive indices of their constituent periodically arranged materials [1]. This FCPBG property is invariably the principle aim of their design. It comes at a significant cost, however, in terms of limited available sample size, the costly fabrication technique required and, most importantly, the absolute requirement to use ultra-high refractive index materials.

Where quasi-ordered PCs have been synthetically fabricated [6, 7] their design has been limited to systems with no more than 12-fold rotational symmetry. This has only marginally reduced the requirement for use of such ultra-high index materials to create the FCPBG properties.

The *E. magnificus* system described in this paper provides a quantified point of reference with which synthetic PCs may be designed to exhibit the visual equivalent of FCPBG properties (namely angle-independent reflected colour) using materials with relatively low refractive index contrast. This has implications for synthetic PC fabrication where high index-contrast materials are inappropriate or unavailable.

The quantification aspect of this work, and indeed its inherent novelty, lies in the discovery and detailed measurement of the numerical extent of quasi-order in the *E. magnificus* PC system. We performed entropy analyses both on its ordered and its quasi-ordered intra-scale structures. While the entropy value (S_y) calculated for the ordered structure was low, entirely as expected, the entropy value calculated for the structure forming the quasi-ordered PC, was $S_b = 0.66$. This may be considered as reference point for synthetic quasi-ordered PC fabrication. The optical performance of an equivalently quasi-ordered synthetic PC, using only low index-contrast materials, is physically predictable both from this naturally evolved system and the measurements and description we present here.

The two types of scale in *E. magnificus* produce the same overall non-iridescent effect for the two different coloured regions using alternative forms of PC. This work outlines contrasting biological methods for production of similar optical effects and offers insight into the costs and benefits of quasi-ordered photonic crystal design from the perspective of bio-inspiration.

Acknowledgements

We thank B.D. Wilts and H.L. Leertouwer for assistance in the experiments and I. R. Hooper for assistance with the programming. Financial support was given by AFOSR/EOARD grant no. FA8655-08-1-3012 and AFOSR grant no. FA9550-10-1-0020, and by the School of Physics at The University of Exeter.